Fuel 158 (2015) 891–897

Contents lists available at ScienceDirect

Fuel

journal homepage: www.elsevier.com/locate/fuel

Co-benefit of Ag and Mo for the catalytic oxidation of elemental mercury

Songjian Zhao [a,1], Zhen Li [b,1], Zan Qu [a], Naiqiang Yan [a,*], Wenjun Huang [a], Wanmiao Chen [a], Haomiao Xu [a]

[a] School of Environmental Science and Engineering, Shanghai Jiao Tong University, 800 Dong Chuan Road, Shanghai 200240, PR China
[b] School of Life Sciences and Biotechnology, Shanghai Jiao Tong University, 800 Dong Chuan Road, Shanghai 200240, PR China

HIGHLIGHTS

- The doped silver can significantly improve Hg^0 oxidation efficiency.
- Ag(2%)–Mo–Ti catalyst had high oxidation efficiency when O_2 was inexistence.
- Ag(2%)–Mo–Ti had a superior resistance toward sulfur dioxide.
- The role of silver on the Hg^0 oxidation process was discussed.

GRAPHICAL ABSTRACT

The mechanism of Hg^0 oxidation by catalyst at a low temperature.

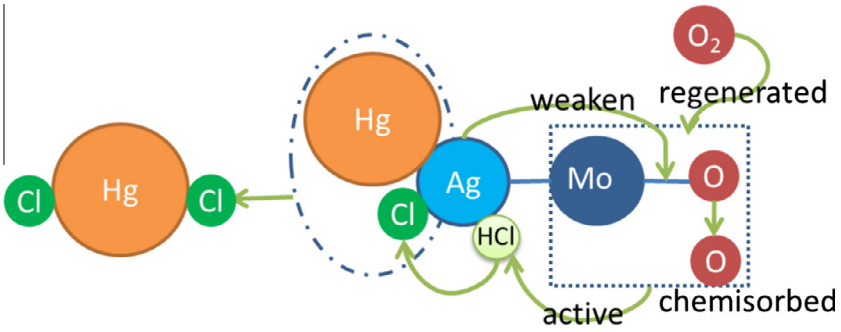

ARTICLE INFO

Article history:
Received 6 January 2015
Received in revised form 14 May 2015
Accepted 16 May 2015
Available online 29 May 2015

Keywords:
Elemental mercury
Catalytic oxidation
Silver

ABSTRACT

The performance of catalyst-combining silver (Ag) and molybdenum (Mo) for elemental mercury (Hg^0) oxidation was clearly improved, and the experimental results demonstrated the synergy between Ag and Mo. The physical and chemical characterizations indicated that Ag^0 and Ag_2MoO_4 nanoparticles existed on the surface of TiO_2 for Ag(2%)–Mo–Ti. Furthermore, the oxidation ability of Mo–Ti was enhanced, and the redox temperature decreased after silver was added. The gas component analysis demonstrated that HCl was the main catalytic component, and the catalyst still had high oxidation efficiency when O_2 was nonexistent. Ag(2%)–Mo–Ti had a superior resistance toward SO_2. Furthermore, Hg^0 breakthrough, desorption, and HCl pretreated experiments were conducted to investigate the catalytic mechanisms of Hg^0 oxidation. The results indicated that Ag had an absorbency role on HCl and Hg^0, and Mo and chemical adsorption oxygen had a catalytic effect on HCl. Adsorbed active Cl subsequently reacted with adsorbed Hg^0 followed by the Langmuir Hinshelwood mechanism at low temperature.

1. Introduction

Mercury emitted from coal-fired power plants has raised considerable concern because of its volatility, persistence, and bioaccumulation in the environment. Mercury was listed as a hazardous and toxic pollutant under Title III of the 1990 Clean Air Act Amendments (CAAA) in the United States [1]. To protect human health and the environment from mercury emissions, the Environmental Protection Agency (EPA) updated the emission limits for new power plants under the Mercury and Air Toxics Standards (MATS) on March 28, 2013. Over 140 nations agreed to sign the Minamata Convention on controlling global anthropogenic mercury emissions in 2013, as well [2]. China was regarded as one of the largest contributors to global, anthropogenic atmospheric

* Corresponding author. Tel./fax: +86 21 54745591.
E-mail address: nqyan@sjtu.edu.cn (N. Yan).
[1] These two authors contributed equally to this work.

http://dx.doi.org/10.1016/j.fuel.2015.05.034
0016-2361/

mercury emissions, accounting for roughly 27% of total [3,4]. Among these mercury emission sources, coal-fired power plants are a major contributor because of the large coal consumption for power generation [5]. Therefore, it is imperative to make strong efforts to reduce mercury emissions from coal-fired power plants.

Mercury emitted from coal-fired flue gas can be classified into three forms: elemental mercury (Hg^0), oxidized mercury (Hg^{2+}) and particulate-bound mercury (Hg^p) [6]. Hg^0, which is the main component of mercury in the gas phase and is notably difficult to remove from the environment due to its high volatility and low solubility in water [7]. However, Hg^{2+} has much higher solubility in water; therefore, the oxidation of Hg^0 to Hg^{2+} followed by the use of typical air pollution control devices, such as ESPs and wet-FGD, is a promising method for mercury removal [8]. To date, great efforts have been undertaken to develop various types of catalysts for mercury oxidation [9].

Molybdenum trioxide (MoO_3) is one of the most important transition metal oxides due to its rich chemistry that is associated with multiple valence states and its high thermal and chemical stability [10]. MoO_3 is widely applied in, for instance, catalysts, sensors, photochromic and electrochromic materials, electrochemical devices, and recording media [11,12]. While molybdenum is frequently added as a promoter to vanadium-based catalysts in the selective catalytic reduction (SCR) of NOx [13] and in Hg^0 oxidation [14], its catalytic oxidation activity is poor.

Silver has been recognized and is often used as an effective catalyst [15,16]. Ag can generate electrophilic oxygen, which facilitates the redox process [7]. Furthermore, adding elemental silver weakens the bond strength between oxygen and metal, thereby explicitly decreasing the activation energy values of the desorption of surface oxygen species [17]. Regarding Hg^0 removal, silver is recognized as an efficient adsorbent for the capture of Hg^0 at low temperature by an amalgamation mechanism. Additionally, Ag and molybdenum can be combined to generate Ag_2MoO_4, which is an important catalyst used in the photocatalytic field [18,19]. Therefore, adding sliver to modify molybdenum is useful for enhancing the oxidation ability of Mo for Hg^0 catalytic oxidation.

In this study, a series of catalysts were prepared and characterized using an X-ray diffractometer (XRD), transmission electron microscopy (TEM), H_2 temperature programmed reduction (H2-TPR), and X-ray photoelectron spectroscopy (XPS). Next, the Hg^0 oxidation efficiency of the Ag-modified Mo–Ti catalyst at low HCl concentrations was investigated. The effect of the flue gas components on Hg^0 oxidation was also examined. Finally, the catalytic mechanisms involved in improving the efficiency at various temperatures were discussed.

2. Experimental section

2.1. Preparation of catalysts

Mo–TiO_2, Ag–TiO_2, Ag–Mo–TiO_2 were prepared by the impregnation method. Appropriate amounts of P25 and $(NH_4)_6Mo_7O_{24}{\cdot}4H_2O$ were mixed and stirred for 1 h, marked as A solution. The mixed solution of PVP and $AgNO_3$ precursor was stirred for 6 h at room temperature, marked as B solution. B solution was added by drops into A solution and stirred constantly for 2 h. Next, the mixed solution was evaporated and dried with a rotary evaporation apparatus (RE-52AAA, Shanghai) and finally calcined in a muffle furnace for 5 h at 500 °C. The Mo–TiO_2, Ag–TiO_2 and Ag–Mo–TiO_2 catalysts are abbreviated as Mo–Ti, Ag–Ti and Ag–Mo–Ti. The element proportions of Ag and Mo to TiO_2 are based on the atomic percentages, i.e., Ag(*x*%)–Ti represents the Ag/TiO_2 mole ratio, and 1% was omitted. The preliminary experiment indicated that 2% Ag was appropriate for Ag(1%)–Mo–Ti, Ag(2%)–Mo–Ti and Ag(3%)–Mo–Ti due to the higher Hg^0 oxidation efficiency.

2.2. Catalytic activity evaluation

The catalytic activity of the as-prepared samples was evaluated in accordance with the previously described criteria [7], including data for a simulated gas preparation system, a catalytic reaction device, a cold vapor atomic absorption spectrometer (CVAAS) and an online data acquisition system. The simulated gas system and the catalytic reaction device included eight mass flow controllers to prepare the simulated flue gas compositions and a fixed-bed reactor (a quartz tube with the inner diameter of 6 mm and a tube-type resistance furnace). The catalyst (40–60 meshed particles) was filled in a quartz tube and fixed with quartz wool. Hg^0 vapor was prepared from an Hg^0 permeation unit and was blended with the gases before they entered the reactor. The concentration of Hg^0 in the gas was analyzed using a mercury analyzer (CVAAS SG-921).

At the beginning of each test, the gas containing Hg^0 initially passed through the bypass without a catalyst; it was subsequently sent to the CVAAS to determine the baseline. When the concentration of Hg^0 was maintained within ±5% for more than 30 min, the gas was diverted to the fixed-bed reactor with the catalysts. Until the catalysts were saturated, 5 ppm HCl was passed in the apparatus to estimate the oxidation efficiency of the Hg^0. The gas flow rate was 30 L/h, corresponding with a space velocity (SV) of $4.26 \times 10^5\ h^{-1}$. N_2 was used as the carrier gas, and the oxygen content was 4%. Because the catalysts were first saturated in 300 μg/m^3 Hg^0 and the N_2/O_2 gas flow, the Hg^0 concentration decrease across the catalysts after passing the HCl was attributed to Hg^0 oxidation. Accordingly, the definition of Hg^0 oxidation efficiency (Eoxi) over the catalysts is as follows:

$$\text{Eoxi}\ (\%) = \frac{\Delta Hg^0}{Hg^0_{in}} = \frac{Hg^0_{in} - Hg^0_{out}}{Hg^0_{in}}$$

The temperature programmed desorption curves of Hg proceeded as follows: a known amount of adsorbents were placed in the adsorption device with N_2 + 4% O_2 at 30 L/h and 100 °C to adsorb mercury for 2 h. Afterwards, the oxygen flow was stopped, a nitrogen flow began, and the Hg signal curve was recorded at 2 °C/min until the temperature reached 450 °C.

2.3. Characterization of the catalysts

The crystalline structure was determined using an X-ray diffraction-meter (APLX-DUO, BRUKER, Germany) between 10° and 80° at a step of 7°/min using Cu Ka radiation (40 kV and 20 mA). The catalyst microstructure was analyzed by transmission electron microscopy (TEM) (JEM-2010HT). The sample was dispersed in ethanol with strong sonication before analysis. Hydrogen temperature programmed reduction (H_2-TPR) experiments were performed on a Chemisorp TPx 2920 instrument, and the catalysts were degassed at 200 °C for 3 h under Ar at atmosphere before the H_2-TPR test. The reducing gas was 10% H_2/Ar. The X-ray photoelectron spectroscopy (XPS) measurement was completed with an AXIS UltraDLD (Shimadzu-Kratos) spectrometer with Al Ka as the excitation source. The C1s line at 284.8 eV was taken as the reference for the binding energy calibration.

3. Results and discussion

3.1. Comparison of the catalytic performance of various catalysts

Fig. 1 shows the comparison of the catalytic performance of various catalysts at various temperatures with a $4.26 \times 10^5\ h^{-1}$ space velocity after passing through the 5 ppm HCl. Ag(2%)–Ti and Mo–Ti exhibited little activity toward Hg^0 oxidation compared with that

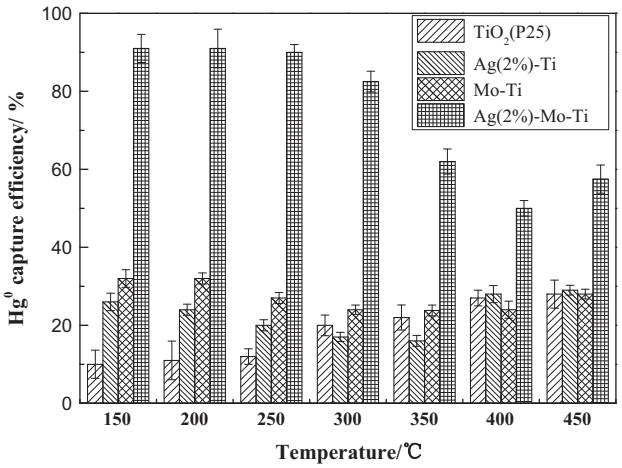

Fig. 1. Catalytic performance of various catalysts at various temperatures with $4.26 * 10^5\ h^{-1}$ space velocity after passing 5 ppm HCl.

of TiO_2, as demonstrated by the poor Hg^0 oxidation performance of Ag or Mo. When Ag and Mo were combined, the catalytic activity significantly improved whether at low or high temperature, as indicated by the synergy between Ag and Mo. However, the catalytic performance of Ag(2%)–Mo–Ti was reduced when the temperature increased, indicating that the catalytic activity of Ag(2%)–Mo–Ti was better at low temperature, which was suitable for oxidizing Hg^0.

3.2. The physical and chemical characterization

To obtain the microscopic morphology information of the catalysts, transmission electron microscopy (TEM) analyses of the Mo–Ti and Ag(2%)–Mo–Ti nanoparticles were performed, as shown in Fig. 2. The TEM image in Fig. 2(a) exhibits evenly distributed Mo–Ti nanoparticles with diameters of 30–40 nm. The high-resolution transmission electron microscopy (HRTEM) results shown in Fig. 2(b) further confirmed the crystalline structure of Mo–Ti. As seen from the figure, the interplanar spacing of 0.347 nm and 0.35 nm corresponded to MoO_3 (040) and TiO_2 (101) [7,20], respectively, indicating that molybdenum was loaded onto the surface of TiO_2 and existed in the form of MoO_3. Fig. 2(c) shows the TEM image of Ag(2%)–Mo–Ti. Some small Ag nanoparticles were attached on the surface of TiO_2 as shown in the figure. The HRTEM in Fig. 2(d) shows interplanar spacing of 0.209 nm, 0.35 nm and 0.33 nm, which were attributed to the TiO_2 (004), TiO_2 (101) and Ag_2MoO_4 (2–20) [21,22], respectively, and manifested the existence of Ag_2MoO_4 on the surface of support.

To identify the crystallographic structure of Ag(2%)–Mo–Ti, the X-ray diffraction (XRD) was characterized, and the elemental content of Ag and Mo was increased to 5% because the low content signal was scarcely detected. Fig. 3 presents the XRD patterns of the various catalysts calcined at 500 °C, and the anatase and rutile phases of TiO_2 were clearly observed from all the catalysts in the figure. In addition, the peaks of Ag^0 are seen in Fig. 3(a), which indicated that the metal state of silver existed on the support structure [23]. The peak of MoO_3 was weak in Fig. 3(b) [24], indicating that either MoO_3 was well-dispersed on the TiO_2 surface or the

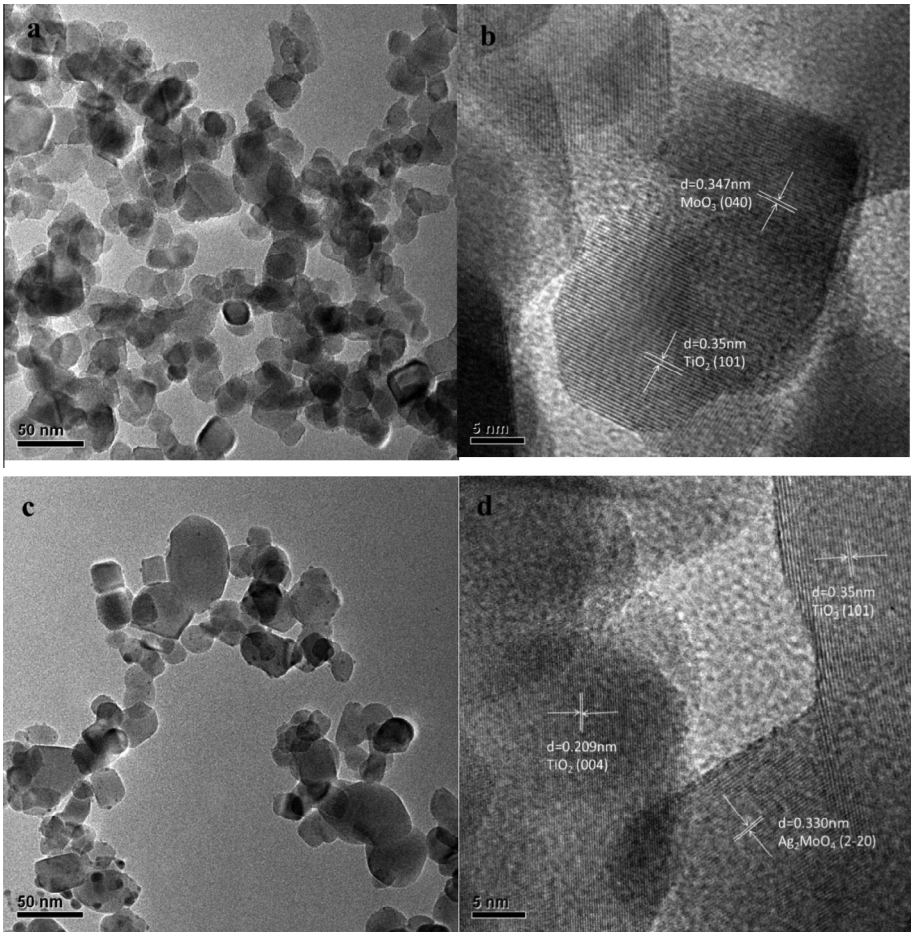

Fig. 2. TEM and HRTEM images: Mo–Ti (a and b) and Ag(2%)–Mo–Ti (c and d).

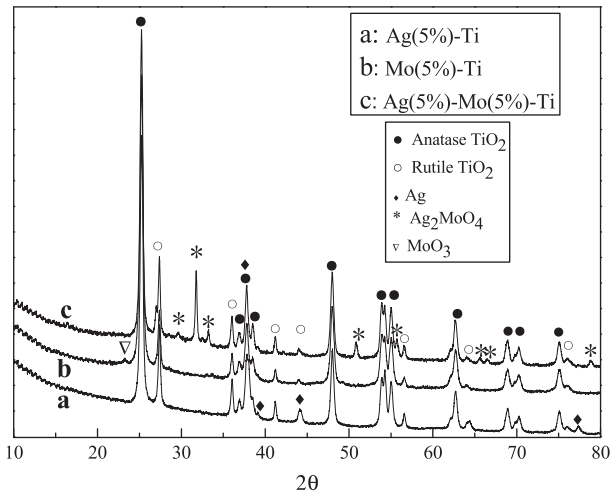

Fig. 3. XRD patterns of various catalysts calcinated at 500 °C.

crystallinity was inferior. There were characteristic peaks of Ag_2MoO_4 in Fig. 3(c), which indicated that silver could combine with molybdenum to form Ag_2MoO_4, and Ag_2MoO_4 was stable after it was calcined [25]. Furthermore, the peak of metal Ag was found for Ag(5%)–Mo(5%)–Ti, illustrating that silver existed in the Ag^0 and Ag_2MoO_4 mixture, consistent with the TEM results.

Fig. A1 presents the TPR profiles of the various catalysts. As seen from this figure, p25 had no obvious peak, and the oxidation ability was weak. When silver was added, there was a peak at 150 °C, which was attributed to the reduction of Ag^+ on the support structure [7]. Four peaks were clearly observed in Fig. A1(c), and the peaks at approximately 380 °C, 580 °C and 680 °C corresponded to the reduction of MoO_3 to MoO_2, while the peak at roughly 780 °C represented the reduction of MoO_2 to Mo metal [26]. The reduction temperature was significantly decreased compared with the two reduction peaks at 733–737 °C and 861–890 °C for the bulk MoO_3 that corresponded to the two-step reduction of MoO_3 ($MoO_3 \rightarrow MoO_2 \rightarrow Mo^0$) [27], which is likely the consequence of the interaction between molybdenum oxide and TiO_2. The reduction peak of MoO_3 to MoO_2 obviously shifted to a lower temperature in Fig. A1(c), indicating that either the oxidation ability of the catalyst was enhanced due to the synergy between Ag and Mo or the bond strength of Mo–O weakened [17,28].

Fig. 4 shows the XPS spectra of Mo–Ti and Ag(2%)–Mo–Ti over the spectral regions of Mo 3d, Ag 3d, Cl 2p and Hg 2p; it also shows the Mo 3d XPS spectrum. The peaks located at 232.9 eV and 236.0 eV were attributed to Mo 3d5/2 and Mo 3d 3/2 electronic state of Mo^{6+}, respectively, and the peaks at 231.5 eV and 234.7 eV were attributed to the presence of Mo^{5+} [29]. As seen in Fig. 4(a), Mo existed in the mixture of Mo (V) and Mo (VI) states for Mo–Ti, and when silver was added, the characteristic peaks of Mo 3d shifted slightly to the high binding energy. This result indicated that the high valence amount of molybdenum was increased to be beneficial for the catalyst oxidation ability. After reaction, the characteristic peaks slightly shifted to the low binding energy, which occurred because Mo^{6+} participated in the reaction that oxidized HCl or Hg^0. Finally, it can be concluded that HCl was not adsorbed on the surface of the molybdenum because the intensity of the Mo 3d peak was not weakened.

Fig. 4(b) recorded the Ag 3d XPS spectrum. The peaks at 367.90 eV and 373.94 eV were attributed to Ag (I), and those at 368.23 eV and 374.09 eV were attributed to metallic silver Ag (0) [7]. Obviously, the silver nanoparticles were present in the metallic silver (Ag^0) and Ag^+ (AgO or Ag_2MoO_4) mixture, and metallic silver was dominant. After this reaction, the intensity of the characteristic peaks weakened and existed mainly in the form of Ag^+. This phenomenon occurred because the HCl was adsorbed on the surface of Ag followed by the HCl activation by the molybdenum and the active oxygen to activate Cl. An amount of Ag^0 was oxidized to Ag^+ and was beneficial to generate electrophilic oxygen to further oxidize Mo^{5+} to Mo^{6+} [7].

The O 1s XPS spectrum is shown in Fig. 4(c). The characteristic peak at 529.8 eV may be ascribed to lattice oxygen, and the peak at 531.4 eV may be attributed to the surface chemisorbed oxygen. When adding silver, the proportion of chemisorbed oxygen increased, beneficial for the Hg^0 oxidation. After reaction for about 10 h, the amount of chemisorbed oxygen quantity decreased, suggesting that chemisorbed oxygen participated in the reaction. However, chemisorbed oxygen still existed on the surface of catalyst, which might be replenished by the lattice oxygen or the gaseous oxygen.

The XPS Cl 2p spectra is shown in Fig. 4(d). There were two peaks at 197.8 eV and 199.7 eV for Cl 2p, which were attributed to the ionic (Cl^-) and covalent (–Cl) chlorine species, respectively [30]. The ionic chlorine (Cl^-) may be the $HgCl_2$ generated by the reaction of the chlorine species and mercury or some amount of AgCl. Moreover, the covalent (–Cl) chlorine species might be the adsorbed HCl or the active Cl.

The Hg 4f XPS patterns are shown in Fig. 4(e). The characteristic peak could not found for Hg 4f from Fig. 4(e), which was due to the smaller Hg content, indicating that the reaction produced little $HgCl_2$ that was adsorbed on the surface of Ag(2%)–Mo–Ti and that most of the compound entered the flue gas.

3.3. The gas components analysis

Fig. 5 shows the Hg^0 catalytic oxidation efficiencies of Ag(2%)–Mo–Ti for the various test cases. It can be observed that the Hg^0 oxidation efficiency was low in the condition of N_2 or the mixture of N_2 and O_2 for Ag(2%)–Mo–Ti, indicating that O_2 was not the main oxidation component for the Hg^0 catalytic oxidation. When HCl was passed, the oxidation efficiency was high, regardless of whether O_2 existed or not. It was determined that HCl was important for the Hg^0 catalytic oxidation, and active Cl or Cl_2 would be generated by the catalysis of Ag(2%)–Mo–Ti. It was reported that O_2 was necessary for Hg^0 oxidation by HCl [31], besides, based on the analysis of O 1s XPS, speculated that chemical adsorption oxygen participated in the reaction. However, the catalyst still had high oxidation efficiency when O_2 was nonexistent, so we speculated the lattice oxygen was transferred to chemical adsorption oxygen at the beginning reaction stage, and the lattice oxygen was active. Meanwhile, on account of the analysis of TPR, we thought that the Mo–O bond was weaken, chemical adsorption oxygen and Mo^{6+} could also easily participate in the reaction to oxidize HCl into active Cl. When 500 ppm sulfur dioxide was added, the Hg^0 catalytic efficiency was still high, indicating that Ag(2%)–Mo–Ti had a superior resistance toward SO_2. The efficiency improved when adding 500 ppm nitric oxide, indicating that NO promoted the Hg^0 oxidation, consistent with similar research [5]. Furthermore, 4% water slightly inhibited the Hg^0 oxidation reaction.

3.4. The catalytic oxidation Hg^0 mechanism analysis

To understand the mercury combination property of the catalysts, Hg^0 adsorption and desorption experiments were performed. Fig. A2(a) shows the Hg^0 breakthrough curves over Ag(2%)–Mo–Ti at various temperatures. As seen in Fig. A2(a), Hg^0 could be adsorbed on the surface of Ag(2%)–Mo–Ti at 150 °C; However, with the increasing temperature, the concentration of Hg^0 was continuously high, indicated that Hg^0 was hardly adsorbed on the surface

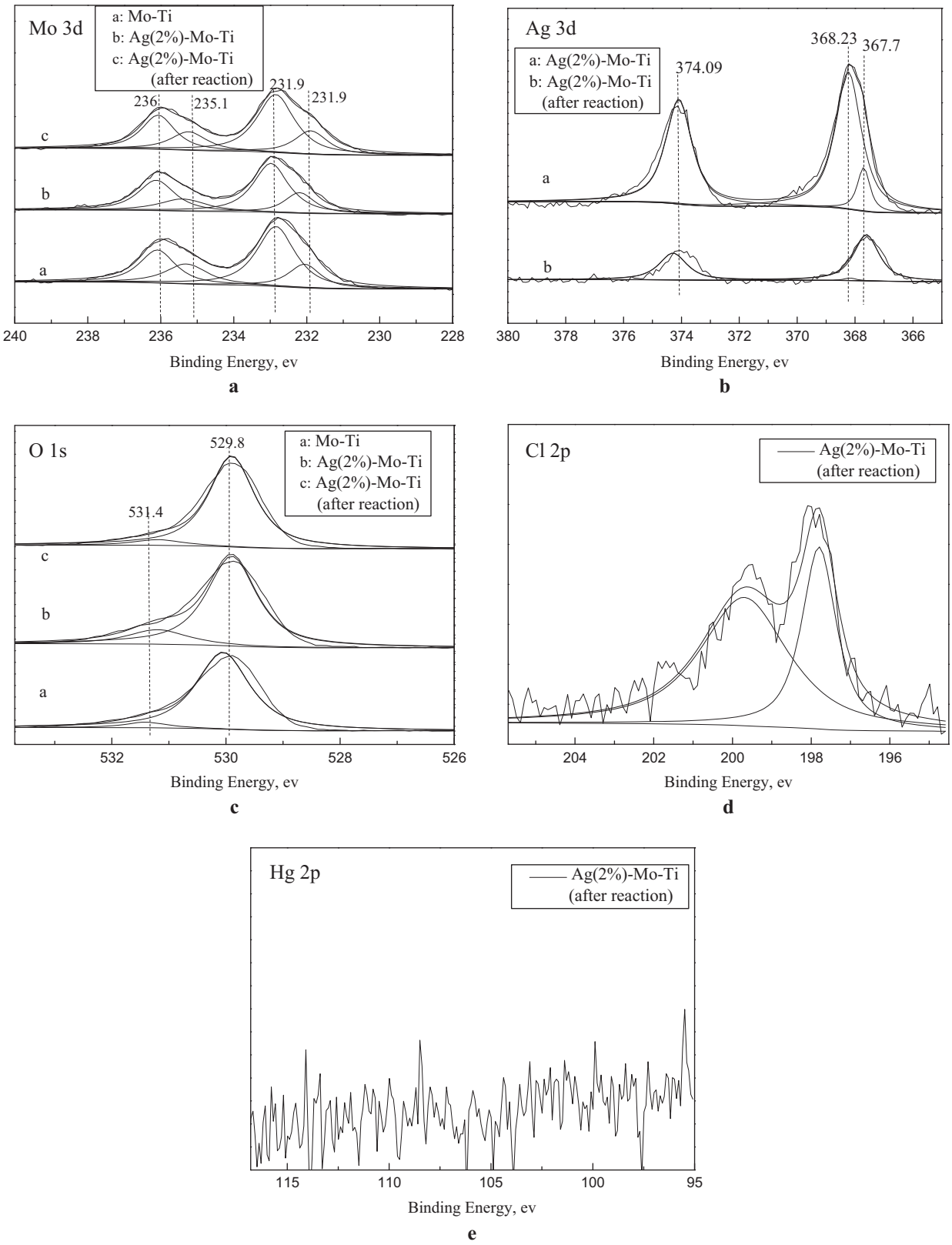

Fig. 4. XPS spectra of Mo–Ti and Ag(2%)–Mo–Ti over the spectral regions: Mo 3d (a), Ag 3d (b), O 1s(c), Cl 2p (d) and Hg 2p (e).

of the catalyst at high temperature. So, the mechanism of Hg^0 oxidation at low and high temperature was different.

The Hg-TPD curves for Ag(2%)–Mo–Ti are shown in Fig. A2(b). It can be observed from Fig. A2(b) that there was little Hg^0 desorbed from Mo–Ti, revealing that the Hg^0 was hardly adsorbed on the surface of Mo or Ti. So, it was difficult for Hg^0 to form a chemical bond between Mo and Ti. Hg^0 was, however, desorbed for Ag(2%)–Ti in the temperature range of 100–250 °C, which was

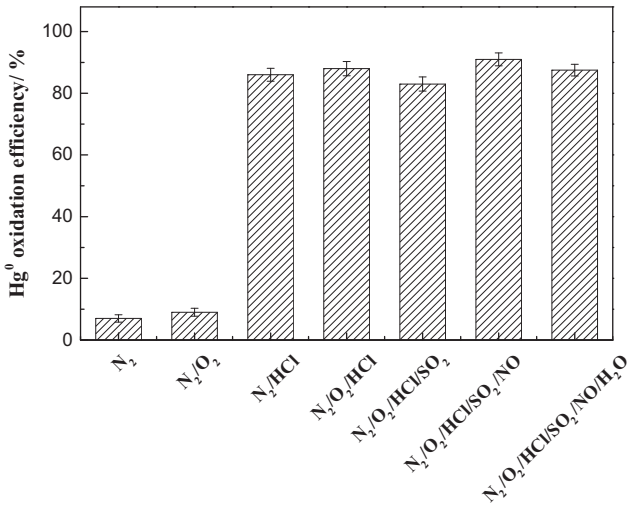

Fig. 5. The Hg^0 catalytic oxidation efficiencies of Ag(2%)–Mo–Ti for various cases.

the decomposition of the silver amalgam. There was little desorbed Hg^0 above 250 °C, indicating that Hg^0 was hardly adsorbed on the surface of the catalyst at high temperature, in accordance with the results of Fig. A2(a). For Ag(2%)–Mo–Ti, Hg^0 could also be desorbed with the increasing temperature; however, the amount of desorbed Hg^0 was less than that of Ag(2%)–Ti. These results indicated that some Ag combined with Mo to form Ag_2MoO_4, as shown by the XRD, and they also suggested the Hg^0 adsorbed component was Ag^0.

To clarify the role of chlorine, an breakthrough experiment using Hg^0 pretreated with HCl was conducted. The experiment proceeded as follows: the Hg^0 passed through 20 ppm HCl as the catalyst for 1 h; then, the HCl supply was closed and the sample area was purged with N_2 for 30 min. Finally, Hg^0 passed through Ag(2%)–Mo–Ti where the Hg^0 concentration change was recorded. Fig. A3 shows the Hg^0 breakthrough curves for HCl-pretreated Ag(2%)–Mo–Ti and Mo–Ti. As seen in Fig. A3(a), the catalyst still had oxidation ability when HCl was not passed compared with the results shown in Fig. A2(a). The chlorine species existed and were adsorbed on the Ag(2%)–Mo–Ti to react with Hg^0. Because the catalyst was purged by nitrogen, HCl or Cl_2 were not physically adsorbed on surface of the catalyst, and the existing component for oxidizing Hg^0 was an active chlorine species formed by the reaction between the adsorbed HCl and Ag(2%)–Mo–Ti. The Hg^0 oxidation efficiency was reduced with an increase in temperature, which showed that more chlorine species were adsorbed at low temperature, indicating that the catalyst oxidation ability of Ag(2%)–Mo–Ti was high and generated more active Cl at low temperature. The active Cl was easily adsorbed on the surface of the catalyst at low temperature, as well. However, the catalyst still had Hg^0 oxidation ability at high temperature, and part of the active Cl was also adsorbed on the surface of the catalyst and was present in the flue gas. The combined results of Figs. A2(a) and A3(a) implied that the adsorbed active Cl reacted with the adsorbed Hg^0 followed by a Langmuir Hinshelwood mechanism at low temperature. At high temperature, the active chlorine species adsorbed on the silver nanoparticles, and gas-active chlorine reacted with the gas-phase Hg^0 by the Eley Rideal mechanism and a homogeneous gas phase reaction.

Fig. A3(b) shows the Hg^0 breakthrough curves for HCl-pretreated Ag(2%)–Ti, Mo–Ti and Ag(2%)–Mo–Ti. As seen in Fig. A3(b), the Hg^0 oxidation efficiency of Ag(2%)–Ti and Mo–Ti was low, indicating a small amount of active Cl and demonstrating that only Ag or Mo could not catalyze chlorine into active Cl. This occurred because Ag had an adsorption role for HCl, and Mo had a catalytic effect for HCl, as shown by the XPS results. The combination of Ag and Mo efficiently oxidized the HCl into active Cl, and the adsorbed active oxygen participated in the reaction. Therefore, Ag(2%)–Mo–Ti had a higher Hg^0 oxidation efficiency.

Fig. A4 shows the mercury concentration change curves for Ag(2%)–Mo–Ti after adding HCl at 150 °C. The concentrations of total mercury (Hg^t) and elemental mercury (Hg^0) were reduced after the HCl addition, and the Hg^0 concentration was lower than the Hg^t concentration. The gap between Hg^0 and Hg^t was the Hg^{2+} concentration, indicating that Hg^0 could be oxidized by Ag(2%)–Mo–Ti and that HCl was the major catalytic component. The total mercury concentration was reduced, which might be that a small amount of $HgCl_2$ that was adsorbed on the surface of the catalyst.

Based on the above results, the main reaction process for Hg^0 oxidation over Ag(2%)–Mo–Ti at low temperature is shown in Fig. 6. Silver weakened the bond strength of Mo–O, so the lattice oxygen was transferred easily to chemical adsorption oxygen. Mo^{6+} and chemical adsorption oxygen participate in the oxidation reaction by the Mars–Maessen mechanism, which oxidized HCl into active Cl. The presence of gas-phase O_2 regenerated the lattice oxygen and chemical adsorption oxygen, and prompted the process of Mo^{5+} to Mo^{6+}. The active chlorine species and Hg^0 were both adsorbed on the silver nanoparticles and reacted with each other following the Langmuir Hinshelwood mechanism to generate $HgCl_2$.

4. Conclusions

Ag(2%)–Mo–Ti was an excellent catalyst for catalytic oxidation of elemental mercury. When combining Ag and Mo, the catalytic activity of Ag(2%)–Mo–Ti was significantly improved whether at low or high temperature, indicating the synergy between Ag and Mo. The catalytic activity of Ag(2%)–Mo–Ti was enhanced, and it was suitable for oxidizing Hg^0 at low temperature. The characterization results indicated that Ag^0 and Ag_2MoO_4 nanoparticles

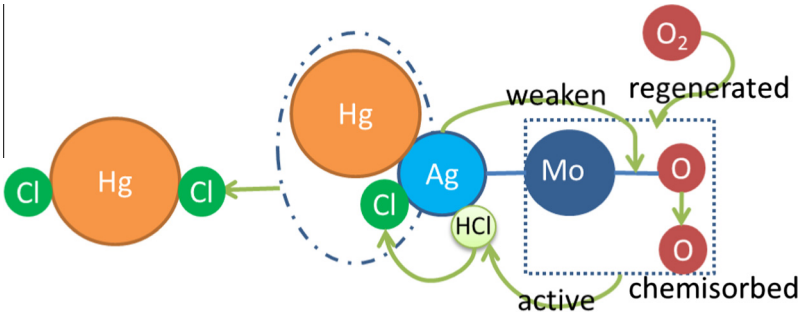

Fig. 6. Reaction process for the Hg^0 oxidation over Ag(2%)–Mo–Ti at low temperatures.

existed on the surface of TiO_2, and the oxidation ability of the catalyst was enhanced due to the synergy between Ag and Mo. Furthermore, the bond strength of Mo–O might be weakened, which is beneficial for the oxidation ability. The gas component effect analysis showed that HCl was the primary catalytic component, and the catalyst still had high oxidation efficiency when O_2 was nonexistent. Additionally, Ag(2%)–Mo–Ti had a superior resistance toward sulfur dioxide, and NO promoted the Hg^0 oxidation; water slightly inhibited the Hg^0 oxidation reaction. Hg^0 breakthrough, desorption and HCl pretreated experiments were performed to study the catalytic mechanisms of the elemental mercury oxidation, which indicated that the adsorbed active Cl reacted with the adsorbed Hg^0 followed by the Langmuir Hinshelwood mechanism at low temperature. Ag had an adsorbent role for HCl and Hg^0. Mo and chemical adsorption oxygen had a catalytic effect for HCl which, when combined with Ag and Mo, could efficiently oxidize HCl into active Cl, indicating that the catalyst had high oxidation ability.

Acknowledgments

This study was supported by the Major State Basic Research Development Program of China (973 Program, No. 2013CB430005), the National Natural Science Foundation of China (Nos. 21277088, 50908145) and the National High-Tech R&D Program (863) of China (Nos. 2013AA065403, 2012AA062504).

Appendix A. Supplementary material

Supplementary data associated with this article can be found, in the online version, at http://dx.doi.org/10.1016/j.fuel.2015.05.034.

References

[1] Gao Y, Zhang Z, Wu J, Duan L, Umar A, Sun L, Guo Z, Wang Q. A critical review on the heterogeneous catalytic oxidation of elemental mercury in flue gases. Environ Sci Technol 2013;47:10813–23.
[2] Liang S, Zhang C, Wang Y, Xu M, Liu W. Virtual atmospheric mercury emission network in China. Environ Sci Technol 2014;48:2807–15.
[3] Pacyna EG, Pacyna J, Sundseth K, Munthe J, Kindbom K, Wilson S, Steenhuisen F, Maxson P. Global emission of mercury to the atmosphere from anthropogenic sources in 2005 and projections to 2020. Atmos Environ 2010;44:2487–99.
[4] Pirrone N, Cinnirella S, Feng X, Finkelman R, Friedli H, Leaner J, Mason R, Mukherjee A, Stracher G, Streets D. Global mercury emissions to the atmosphere from anthropogenic and natural sources. Atmos Chem Phys 2010;10:5951–64.
[5] Yan N, Chen W, Chen J, Qu Z, Guo Y, Yang S, Jia J. Significance of RuO2 modified SCR catalyst for elemental mercury oxidation in coal-fired flue gas. Environ Sci Technol 2011;45:5725–30.
[6] Gao W, Liu Q, Wu C-Y, Li H, Li Y, Yang J, Wu G. Kinetics of mercury oxidation in the presence of hydrochloric acid and oxygen over a commercial SCR catalyst. Chem Eng J 2013;220:53–60.
[7] Zhao S, Ma Y, Qu Z, Yan N, Li Z, Xie J, Chen W. The performance of Ag doped V2O5–TiO2 catalyst on the catalytic oxidation of gaseous elemental mercury. Catal Sci Technol 2014;4:4036–44.
[8] Beretta A, Usberti N, Lietti L, Forzatti P, Di Blasi M, Morandi A, La Marca C. Modeling of the SCR reactor for coal-fired power plants: impact of NH₃ inhibition on Hg⁰ oxidation. Chem Eng J 2014;257:170–83.
[9] Presto AA, Granite EJ. Survey of catalysts for oxidation of mercury in flue gas. Environ Sci Technol 2006;40:5601–9.
[10] Novoselova LY. Mo and MoO3 powders: structure and resistance to CO. J Alloy Compd 2014;615:784–91.
[11] Chiang TH, Yeh HC. A novel synthesis of alpha-MoO3 nanobelts and the characterization. J Alloy Compd 2014;585:535–41.
[12] Wang ZY, Madhavi S, Lou XW. Ultralong alpha-MoO3 nanobelts: synthesis and effect of binder choice on their lithium storage properties. J Phys Chem C 2012;116:12508–13.
[13] Lietti L, Nova I, Ramis G, Dall'Acqua L, Giamello E, Forzatti P, Bregani F. Characterization and reactivity of V2O5–MoO3/TiO2 De-NOx SCR Catalysts. J Catal 1999;187:419–35.
[14] Kamata H, Ueno S-I, Sato N, Naito T. Mercury oxidation by hydrochloric acid over TiO₂ supported metal oxide catalysts in coal combustion flue gas. Fuel Process Technol 2009;90:947–51.
[15] Kou T, Li D, Zhang C, Zhang Z, Yang H. Unsupported nanoporous Ag catalysts towards CO oxidation. J Mol Catal A: Chem 2014;382:55–63.
[16] Yang X, Ma F, Li K, Guo Y, Hu J, Li W, Huo M, Guo Y. Mixed phase titania nanocomposite codoped with metallic silver and vanadium oxide: new efficient photocatalyst for dye degradation. J Hazard Mater 2010;175:429–38.
[17] Ge X, Zhang H-L. Temperature-programmed reduction studies of V–Ag catalysts. J Solid State Chem 1998;141:186–90.
[18] Li ZQ, Chen XT, Xue ZL. Microwave-assisted hydrothermal synthesis of cube-like Ag–Ag2MoO4 with visible-light photocatalytic activity. Sci China Chem 2013;56:443–50.
[19] De Santana YVB, Gomes JEC, Matos L, Cruvinel GH, Perrin A, Perrin C, Andres J, Varela JA, Longo E. Silver molybdate and silver tungstate nanocomposites with enhanced photoluminescence. Nanomater Nanotechnol 2014;4.
[20] Zhang H, Zhuang S, Wu H, Gu S, Lei Y. Effect of carbon nanotubes on the synthesis process of nano-sized Mo powders. Int J Refract Metal Hard Mater 2013;41:370–4.
[21] Yan N, Zhu Z, Zhang J, Zhao Z, Liu Q. Preparation and properties of ce-doped TiO2 photocatalyst. Mater Res Bull 2012;47:1869–73.
[22] Cheng L, Shao Q, Shao M, Wei X, Wu Z. Photoswitches of one-dimensional Ag2MO4 (M = Cr, Mo, and W). J Phys Chem C 2009;113:1764–8.
[23] Wen M, Zhou L, Guan W, Li Y, Zhang J. Formation and bioactivity of porous titania containing nanostructured Ag. Appl Surf Sci 2010;256:4226–30.
[24] Bai SL, Chen C, Zhang DF, Luo RX, Li DQ, Chen AF, Liu CC. Intrinsic characteristic and mechanism in enhancing H2S sensing of Cd-doped alpha-MoO3 nanobelts. Sens Actuators B Chem 2014;204:754–62.
[25] Li Z, Chen X, Xue Z-L. Microwave-assisted hydrothermal synthesis of cube-like Ag–Ag2MoO4 with visible-light photocatalytic activity. Sci China Chem 2013;56:443–50.
[26] Arnoldy P, De Jonge J, Moulijn J. Temperature-programed reduction of molybdenum (VI) oxide and molybdenum (IV) oxide. J Phys Chem 1985;89:4517–26.
[27] Zepeda T, Halachev T, Pawelec B, Nava R, Klimova T, Fuentes G, Fierro J. Hydrodesulfurization of dibenzothiophene over CoMo/HMS and CoMo/Ti-HMS catalysts. Catal Commun 2006;7:33–41.
[28] Hui-Liang Z, Wei Z, Xiang D, Xian-Cai F. A study of catalytic activity, constituent, and structure of V—Ag catalyst for selective oxidation of toluene to benzaldehyde. J Catal 1991;129:426–37.
[29] Cheng X, Yu X, Li B, Yan L, Xing Z, Li J. Enhanced visible light activity and mechanism of TiO2 codoped with molybdenum and nitrogen. Mater Sci Eng B Adv Funct Solid State Mater 2013;178:425–30.
[30] Cao Y, Yu Y, Zhang P, Zhang L, He T, Cao Y. An enhanced visible-light photocatalytic activity of TiO2 by nitrogen and nickel–chlorine modification. Sep Purif Technol 2013;104:256–62.
[31] Li H, Wu C-Y, Li Y, Zhang J. CeO2–TiO2 catalysts for catalytic oxidation of elemental mercury in low-rank coal combustion flue gas. Environ Sci Technol 2011;45:7394–400.